Structurally-Driven Selective Adsorption of Hydrocarbons by Metal Substitution in Isostructural Rare-Earth Metal-Organic Frameworks

Chunyi Li[1], Akriti Sarswat[1], Susan E. Henkelis[2], Tina M. Nenoff[2], Ryan P. Lively[1,*], Jessica M. Rimsza[2,*]

[1] Georgia Institute of Technology, Atlanta, GA 30332, USA

[2] Sandia National Laboratories, Albuquerque, NM 87185, USA

Abstract

The design and realization of highly selective nanoporous materials is necessary to target critical separations across industrial communities. By leveraging pore size, pore shape, and linker functionalization, the design of nanoporous solid adsorbents will enable the rapid production of energy efficient separations materials for high value gas mixtures. This study uses a combination of modeling, synthesis, and gas adsorption testing to investigate a new class of small pore isostructural rare-earth (RE) DOBDC metal-organic frameworks (MOFs) (RE: Pr-, Gd-, Er-, Yb; DOBDC = 2,5-dihydroxyterephthalic acid) and their adsorption selectivity for acetylene/ethylene mixtures. Density functional theory (DFT) simulations identified that selective binding of acetylene over ethylene in the Gd-, Er-, and Yb-DOBDC MOFs was due to hydrogen-bonding between the acetylene and the linker hydroxyl. Adsorption experiments validated the computational results by identifying mechanisms that control the acetylene/ethylene adsorption selectivity and high acetylene adsorption. Furthermore, dynamic column breakthrough experiments with the Gd-DOBDC MOF validated the simulations and indicate that ethylene can be separated from acetylene in a mixture containing 1 vol% acetylene and 39 vol% ethylene (balance argon). The results highlight the complexity of gas binding in functional porous materials and how combining modeling and experiment enables a fundamental understanding of gas-framework interactions that can be leveraged for design of future separation materials.

1. Introduction

Ethylene is the most widely produced petrochemical, with global consumption of over 172 million tons in 2021.[1] It serves as an essential raw material for polymer and chemical production, and the current state-of-the-art production process is via steam-cracking of ethane and naphtha.[2] However, during the process, acetylene is produced as an impurity, at approximately 1 mol % of the product.[3] Reduction of the acetylene concentration to less than a few parts per million is necessary for the ethylene product, as it can poison the catalyst during polyethylene production, cause undesired polymerization, or form solid metal acetylides in the fluid stream.[4, 5]

Currently, acetylene removal from ethylene/acetylene mixtures is achieved via four different processes that suffer from low acetylene selectivity, high energy requirements, and large equipment footprints.[6] However, adsorption using porous materials is an attractive alternative technology for acetylene/ethylene separation due to a lower energy-demand separation process based on selective adsorption of acetylene over ethylene. Among the many porous materials used for light hydrocarbon separation,[7] metal-organic frameworks (MOFs) have tunable pore size, pore functionality, and channel structures that can achieve high adsorption uptake and selectivity necessary for gas separations.[8]

MOFs with small pore windows have separated acetylene through molecular sieving effects, but their narrow pores can lead to low acetylene adsorption uptakes.[5, 9-12] Notably, acetylene adsorption in SIFSIX MOFs has been studied extensively. The SIFSIX MOF family incorporates the SiF_6^{2-} units in the framework to introduce preferential acetylene binding over ethylene and carbon dioxide. SIFSIX-1-Cu has preferential binding to acetylene through cooperative host-guest and guest-guest interactions by ordered assembly in the pore channel. The small linker used in SIFSIX-14-Cu-i forms a size selective framework that excludes ethylene almost completely with an acetylene/ethylene adsorption selectivity of 6000. In SIFSIX-2-Cu-i, a relatively high selectivity of 44.5 is achieved in a 1:99 v/v acetylene/ethylene mixture, attributed to the large heat of adsorption for acetylene from hydrogen bonding between acetylene and SiF_6^{2-}anions.[13-15] This shows that a small sized pore MOF with moderate heats of adsorption can be leveraged to design a MOF for acetylene/ethylene separations.

RE-DOBDC (RE = rare earth, DOBDC = 2,5-dihydroxyterephthalic acid) MOFs are a recently explored class of MOFs that show exceptional selectivity and durability to acid gases.[16, 17] Prior studies have shown that this class of MOFs retains the same structure across the lanthanide

series, and that the pore window and pore volume can be tuned by the ionic radius of the incorporated rare earth metal.[17-20] Additionally, variation in binding energies of acid gases (NO_2, SO_2) was previously investigated across the a lanthanide DOBDC MOF series and found to be sensitive to ligand-metal coordination in both periodic and gas-phase density functional theory (DFT) simulations[21] .

Here, we utilize a combined multidisciplinary effort of modeling, synthesis, and gas adsorption testing to understand the structural parameters that govern acetylene/ethylene separations using RE-DOBDC MOFs. The effect of pore size, pore shape, and pore functionality, along with hydrogen bonding and steric hindrance on acetylene/ethylene separations were analyzed. The MOFs were synthesized with DOBDC linkers and metals praseodymium (Pr), gadolinium (Gd), erbium (Er), and ytterbium (Yb) to cover the range of rare earth element ionic radii and evaluate the impact of structural variation of acetylene/ethylene adsorption. Control of the RE-DOBDC MOF structure by incorporation of varying rare earth elements enables investigation of the acetylene/ethylene adsorption equilibrium uptake and gas adsorption to identify the source of variation in selectivity.

2. Materials and Methods

2.1 Computational Methods

For calculated gas adsorption geometries, ground state electronic structures were optimized using spin-unrestricted density functional theory (DFT) simulations as implemented in the Vienna Ab initio Simulation Package (VASP)[22, 23] code in a plane wave basis set,[24] with projector-augmented wave (PAW) potentials.[25, 26] Large core potentials (LCPs), which represent the M(III) oxidation state and place the Ln 4f electrons in the potential core, with a 600 eV cutoff energy and converged to a force accuracy of 0.03 eV/Å, were used with a γ point for k-point sampling. A Gaussian smearing of 0.01 eV was used for smearing of the electron occupation. The generalized gradient approximation (GGA) exchange correlation functional of Perdew–Burke–Ernzerhof designed for solids and surfaces (PBEsol)[27] was chosen for consistency with recent successes in RE-MOFs. [16, 19, 28] The DFT-D3 method of Grimme et al.[29] with Becke–Jonson damping[30] was added as a dispersion correction.

Based on previous studies, the following computational procedure was used as a reproducible process for optimizing RE-DOBDC MOF structures when interchanging metals in the framework.

[16, 28, 31] Initial geometries for the current calculation set were taken from previously reported bi-dentate bound RE-DOBDC MOF structures.[17] Four different RE-DOBDC MOF structures were generated with M = Gd, Yb, Er, and Pr. The structural relaxation of RE-DOBDC MOFs is a multistep process consisting of (1) optimization of atomic positions, (2) optimization of cell volume and atomic positions, and (3) re-optimization of only the atomic positions. Recent reports have indicated that the metal center includes fluorine instead of μ_3–O groups from synthesis with a fluorine-containing modulator.[20, 32] Here, both the completely fluorinated and μ_3–O versions were simulated and the final unit cell sizes are included in Table S1. Computational structures were validated via comparison with simulated and experimental x-ray diffraction data, included in the SI as Figures S1-S3. The final energies of the RE-DOBDC MOF structures were calculated in reciprocal space for increased accuracy. Optimization of gas adsorption to the metal sites was completed by placing the ethylene or acetylene molecule within a physisorption distance of 2–3 Å from the metal center. Two different starting positions were considered for the gas molecule, with the molecule being parallel or perpendicular to the metal cluster, with only the lowest energy binding configuration reported. The MOF system containing the gas molecule was then relaxed using the same parameters listed above for the pure MOF system. The binding energies (E_B) of the systems were calculated as $E_B = E_{MOF+gas} - E_{MOF} - E_{gas}$ with E_{MOF} as the energy of the activated MOF and $E_{MOF+gas}$ the energy of the MOF with the adsorbed gas species.[33] Energy of the gas molecule (E_{gas}) was calculated by simulating a single gas molecule in a 20 Å × 20 Å × 20 Å box, consistent with previous methodologies.[17]

2.2 Material Synthesis

All commercial reagents were used without any further purification. The RE-DOBDC MOFs were synthesized solvothermally using previously published procedures.[17, 19] Synthesis conditions for Pr-DOBDC is presented here; conditions for the other analogues are included in the Supporting Information (SI). Praseodymium chloride (0.066 g, 0.188 mmol) and 2,5-dihydroxyterephathlic acid (0.054 g, 0.275 mmol) were dissolved with sonication in N,N-dimethylformamide (4 mL). 2-fluorobenzoic acid (0.576 g, 4.11 mmol) was dissolved in N,N'-dimethylformamide (4 mL) and added to the salt solution. Water (2 mL) and nitric acid (0.6 mL, 3.5 M) were added to the reaction mixture and heated at 125 °C for 120 hr in a 20 mL scintillation vial. The crystals

were collected by filtration, washed with N,N'-dimethylformamide (2 x 50 mL) and water (2 x 50 mL), and then dried on the filter with acetone (50 mL).

2.3 Powder X-Ray Diffraction

X-Ray diffraction measurements were performed on powdered MOF samples on a Malvern PANalytical Alpha-1 Diffractometer with Cu Kα1 radiation (λ = 1.54178 Å) at room temperature, with step size of 0.08° 2θ.

2.4 Single-Component Ethylene Adsorption Experiment

Samples were activated under high vacuum at 120°C for 16 h prior to gas adsorption isotherms measurements. Single-component ethylene adsorption measurements were conducted on a Micromeritics ASAP 2020HD surface area and porosity analyzer at 26°C. We were unable to test pure acetylene isotherms, as our equipment was incompatible with this gas.

2.5 Dynamic Fixed-Bed Breakthrough and Desorption Experiment

Fixed-bed breakthrough experiments were carried out using a premixed acetylene/ethylene/He (1/39.5/59.5, v/v) mixture (Airgas). MOF samples were packed in a Swagelok 316SS tubing with a diameter of ¼ inch and a length of 2 inches. Quartz wool was used to fill the void volume in the tubing. Blank breakthrough experiments were run using quartz wool-filled sample cells to capture the dead volume in the system. Then, MOF samples were loaded in the sample cell and activated *in situ* at 120°C for 16 h under either helium or argon purge. The acetylene/ethylene/He were fed into the sample cell, and the effluent gas composition was measured using an in-line mass spectrometer. After the sample or blank cell was saturated with the feed gas mixture, desorption experiments were conducted using helium purge. Similarly, the desorption experiments were repeated with blank cells. The breakthrough and desorption experiments were conducted at 23 ± 0.5°C.

2.6 Zero-Length Column (ZLC) Experiment for Diffusivity Measurement

The intracrystalline diffusivities of acetylene and ethylene in the RE-DOBDC MOFs were measured by the ZLC method. A small amount (2-4 mg) of MOF sample was set between quartz

wool layers in a Swagelok reducing union. The sample was pre-equilibrated with the analysis gas mixture. The acetylene/ethylene ratio was maintained at 1/39.5 v/v, where the total hydrocarbon concentration was controlled at 5% by mixing inert helium with the feed gas mixture. Typical ethylene product from steam cracking contains 1 vol% acetylene and 99 vol% ethylene, but 39 vol% ethylene was used here for safety reasons. At time zero, the gas flow was switched to pure argon with flowrates varying from 10-35 sccm, and the effluent concentration was measured by a mass spectrometer. The experimental technique is described in detail by Eic, Ruthven, Brandani, and co-workers.[34-36] A diagram for the ZLC setup is shown in Figure S4, and the desorption dynamics are described by detailed equations in Section S1 Zero-length column (ZLC) diffusivity analysis.

3. Results and Discussion

3.1 Single Gas Binding Energies in RE-DOBDC MOFs

Molecular scale modeling of gas binding in the RE-DOBDC MOF was used to identify how composition of the metal alters the gas-MOF interactions. The calculation of acetylene and ethylene binding in the four RE-DOBDC MOFs structures is listed in Table 1. Overall, both acetylene and ethylene are stable inside the RE-DOBDC MOFs with binding energies between -57 kJ/mol and -28 kJ/mol. These binding energies are in the range of previously calculated binding energies of acid gases, including SO_2, NO_2, and H_2O, in RE-DOBDC MOFs.[17, 19] Among the RE-DOBDC structures evaluated, the Pr-DOBDC MOF is the only structure that has stronger ethylene binding (-49 kJ/mol) than acetylene (-44 kJ/mol). In all other cases the acetylene binding is stronger than the ethylene molecule by 18 kJ/mol for the Gd-DOBDC MOF to 8 kJ/mol for the Yb-DOBDC MOF, as seen in Table 1. This difference in binding energies supports a general thermodynamic favorability for adsorption of acetylene over ethylene.

Table 1. Binding energies (kJ/mol) of acetylene (C_2H_2) and ethylene (C_2H_4) molecules in RE-DOBDC MOFs (RE = Pr, Gd, Er, Yb) with μ_3 oxygen (μ_3–O) or fluorinated (F) metal cluster. "Mix" denotes a mixture of 30% μ_3–O and 70% fluorinated metal centers in the MOF as reported in Ref[20]

	Pr-DOBDC			Gd-DOBDC			Er-DOBDC			Yb-DOBDC		
	μ_3–O	F	Mix	μ_3–O	F	Mix	μ_3–O	F	Mix	μ_3–O	F	Mix

C_2H_2	-44	-44	-44	-66	-53	-57	-57	-49	-49	-51	-38	-42
C_2H_4	-49	-49	-49	-45	-37	-39	-32	-39	-37	-29	-37	-35

3.2 Acetylene/Ethylene Binding Sites

Changes in binding strength between the ethylene and acetylene arises from the number and strength of the gas-MOF interactions. Three different interatomic distances were evaluated to capture the variability of gas-MOF binding sites, shown in Table 2. First, M···H distances are used to estimate gas-metal interactions. Next, H···O-H distances are used to identify hydrogen bonding between the gas molecule and the hydroxyl on the DOBDC linker. Note that all these bond lengths fall below the sum of the hydrogen and oxygen van der Waals radius (2.61 Å), within the commonly used definition of a hydrogen bond[37]. Finally, the H···O_c distance is the average distance between the four oxygens that link the DOBDC to the metal cluster and the gas molecule. Representative binding sites for ethylene and acetylene in the Gd-DOBDC MOF are included in Figure 1.

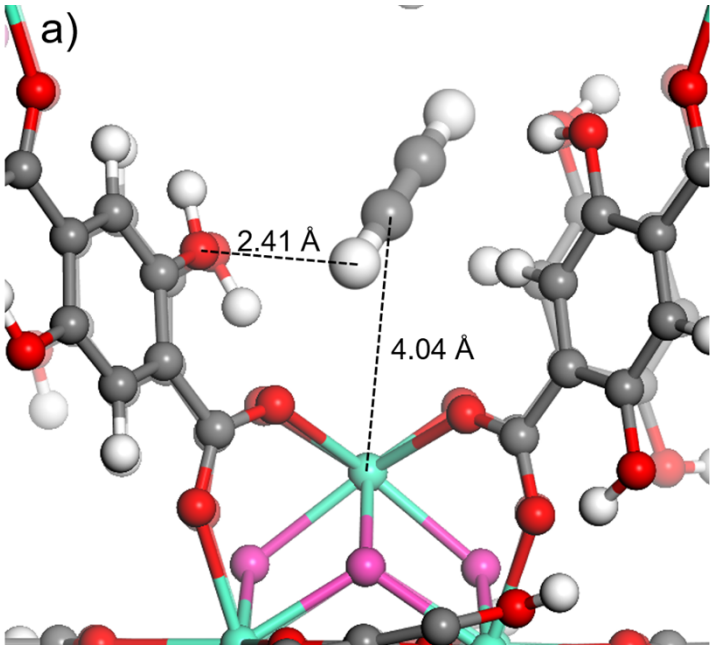

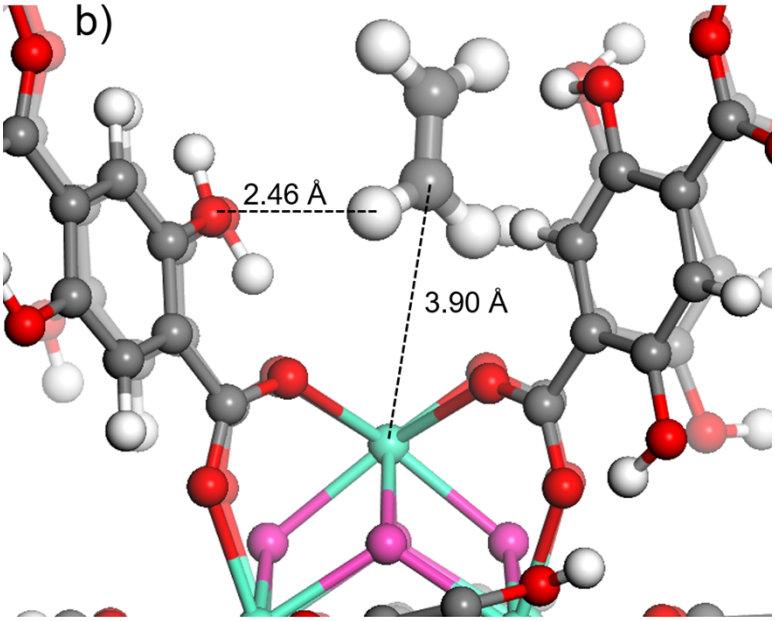

Figure 1: (a) acetylene and (b) ethylene binding in a Gd-DOBDC MOF demonstrating distances and rotation of gas molecule relative to the cluster for acetylene and hydrogen bonding with the hydroxyl on the DOBDC linker. Atom colors: carbon (gray), oxygen (red), fluorine (pink), gadolinium (teal), hydrogen (white)

Analysis of these distances identified the driving factors for gas binding in the RE-DOBDC MOFs. Data in Table 2 highlights that the RE-DOBDC MOFs with preferential acetylene binding exhibit longer M···C and H···O_c distances for acetylene than for ethylene. The result is that the acetylene molecule sits closer to the center of the pore and farther from the metal cluster than ethylene despite its smaller size. Therefore, some other interaction between acetylene and the MOF is causing the increased binding strength.

The source of the stronger acetylene binding is found in the hydrogen bonds between the acetylene and the hydroxyl on the DOBDC linker. As shown in Table 2, the shortest acetylene-MOF bonds arise from the H···O-H distances and are consistently shorter than for ethylene. The sp-hybridized C-H bond in acetylene is a stronger proton donor than the sp2-hybridized C-H bond in ethylene[38], leading to stronger hydrogen bond between acetylene and the hydroxyl on the DOBDC linker. Additionally, the length of the hydrogen bond is linearly correlated with its binding strength, with shorter C···O bond lengths associated with increased hydrogen bond strength[39]. In these RE-DOBC systems, the Yb-DOBDC MOF has a longer H···O-H distance than

the other three RE-DOBDC MOFs, which is balanced by shorter H···O_c distances (3.20±0.41 Å). The longer hydrogen bond distances in Yb-DOBDC MOF supports weaker acetylene binding energies. Two competing binding sites exist in the RE-DOBDC MOFs, one with the hydroxyl on the DOBDC linker that is stronger for acetylene than ethylene, and one interacting with the oxygen linking the DOBDC to the metal cluster that is stronger for ethylene over acetylene.

Table 2: Binding geometries (Å) for acetylene (C_2H_2) and ethylene (C_2H_4) molecules in RE-DOBDC MOFs (RE = Pr, Gd, Er, Yb) including interatomic distances between the molecule and the metal center (M···H), the hydrogen bond length between the gas and a hydroxyl on the neighboring DOBDC linker (H···O-H), and the average and standard deviation of the distance between the gas molecule and the oxygen on the DOBDC linker that connect to the metal cluster (H···O_c).

	M···C				H···O-H				H···O_c			
	Pr	Gd	Er	Yb	Pr	Gd	Er	Yb	Pr	Gd	Er	Yb
C_2H_2	3.73	4.04	4.11	5.44	2.25	2.41	2.28	2.84	3.25 ±0.65	3.28 ±0.59	3.32 ±0.49	3.20 ±0.41
C_2H_4	4.08	3.90	3.89	3.68	2.75	2.46	2.41	2.28	3.14 ±0.51	2.95 ±0.45	2.90 ±0.36	2.68 ±0.31

3.3 Accessibility of the Metal Cluster

Analysis of the O-M-O bond angles in the RE-DOBDC MOFs was used to quantify accessibility of the metal cluster for gas binding, with higher bond angles indicating greater binding site accessibility. The largest O-M-O bond angles were for the Pr-DOBDC MOF with values of 131.8±0.5° and the smallest was for the Yb-DOBDC MOF with O-Yb-O bond angles of 127.9±0.4°. The O-M-O bond angles in the Gd-DOBDC MOF (129.7±0.7°) and the Er-DOBDC MOF (128.6±0.3°) fell in the intermediate range. Snapshots of the metal clusters including these bond angles are included in the Supporting Information as Figure S5. Note that the variation in O-M-O bond angles with μ3-O in the metal clusters was well within the standard error of the parameter. For example, the O-Pr-O bond angle is 131.9±0.5° for the fluorinated Pr-DOBDC MOF compared with 131.8±0.5° for the μ3-O composition.

For ethylene adsorption the gas binding energies follow the trend of largest O-M-O bond angle having the stronger gas binding. The RE-DOBDC MOF with the largest O-M-O bond angle, Pr-DOBDC, has the strongest binding energy of -49 kJ/mol and the RE-DOBDC MOF with the narrowest O-M-O bond angle, Yb-DOBDC having the weakest binding energy of -35 kJ/mol. Binding is by hydrogen bonding between the hydrogen on the ethylene and the oxygen either (i) connecting the DOBDC linker to the metal or (ii) from the hydroxyl groups on the DOBDC with limited direct interaction with the metal center.

For acetylene, three of the four RE-DOBDC MOFs follow the same trend of stronger binding with a larger O-M-O bond angle including the Gd-, Yb-, and Er-DOBDC MOFs. The Pr-DOBDC MOF is an outlier, with a weaker acetylene binding then would be predicted based on the O-M-O bond angle. Further evaluation of acetylene binding structures in the Pr-DOBDC MOF identified that acetylene has two hydrogen bonds by binding with hydroxyl groups from two different DOBDC linkers, as seen in Figure 2. Unlike the ethylene molecule, the acetylene molecule has more rotational freedom when interacting with the MOF structure between DOBDC linkers, which allows the acetylene molecule to form stronger hydrogen-bond structures with multiple hydroxyl groups. Figure 1 includes snapshots of the acetylene in the Gd-DOBDC MOF and demonstrates rotation of the acetylene molecule relative to the two DOBDC linkers. By contrast the ethylene molecule is centered between them. The results highlight the complexity of hydrocarbon interaction inside small pored RE-DOBDC MOFs and how even small variations in isostructural MOFs caused by changing metal composition can have significant impact on the gas adsorption energies.

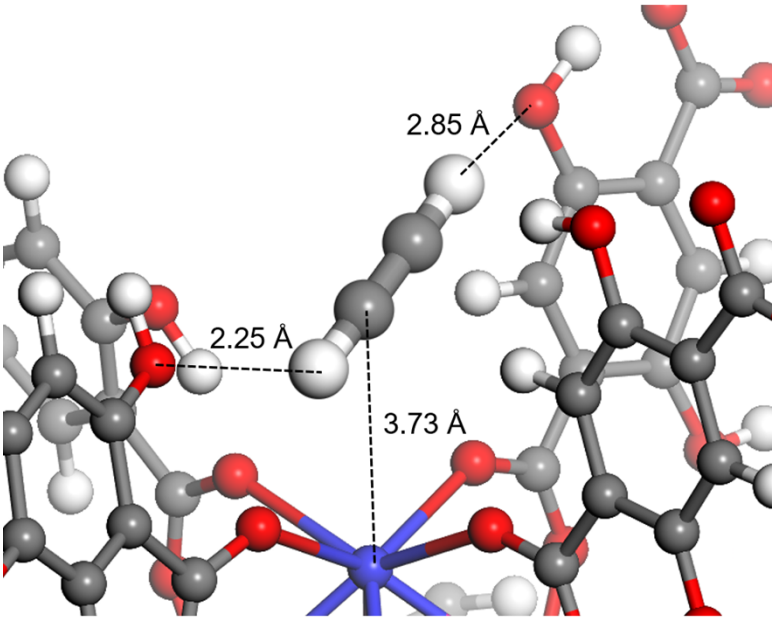

Figure 2: Snapshot of acetylene binding in Pr-DOBDC MOFs via hydrogen bond with two hydroxyl groups on different DOBDC linkers. Atom colors: carbon (grey), oxygen (red), praseodymium (blue), hydrogen (white)

3.4 Single and Multicomponent Experimental Gas Isotherms

Experimental single component ethylene adsorption isotherms were carried out to evaluate the RE-DOBDC MOF adsorption capacity and are included in Figure 3. At partial pressures below 10 kPa, Gd-DOBDC showed the highest ethylene adsorption capacity, followed by the Pr- and Er-DOBDC MOFs, and finally the Yb-DOBDC MOF. However, repeated ethylene isotherm measurements showed that ethylene adsorption in Yb-DOBDC had large variances among measurements, suggesting possible structural change during adsorption and desorption. Due to its inconsistent isotherm measurements, it was not considered further for acetylene/ethylene separation.

To evaluate the effect of MOF structure on gas adsorption and selectivity, the binary adsorption capacities of acetylene and ethylene were measured experimentally using dynamic column breakthrough experiments. The experimental selectivities for a binary acetylene and ethylene mixture were calculated from the binary adsorption capacities. All four of the RE-DOBDC MOFs studied are acetylene-selective from experimental results, with acetylene/ethylene selectivities over one, as shown in Figure 4.

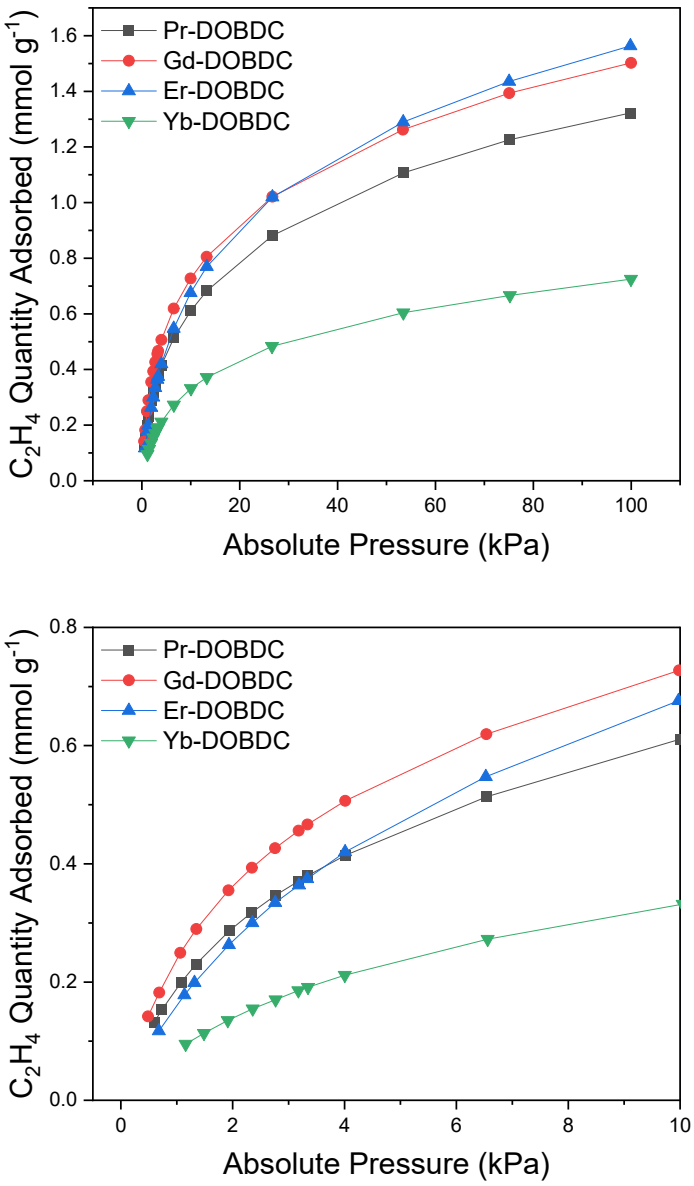

Figure 3. Single-component ethylene adsorption isotherms on Pr-, Gd-, Er-, and Yb-DOBDC at 300K, listed in the order of descending metal ionic radius. The bottom plot is an enlarged section of the isotherms between 0 and 10 kPa.

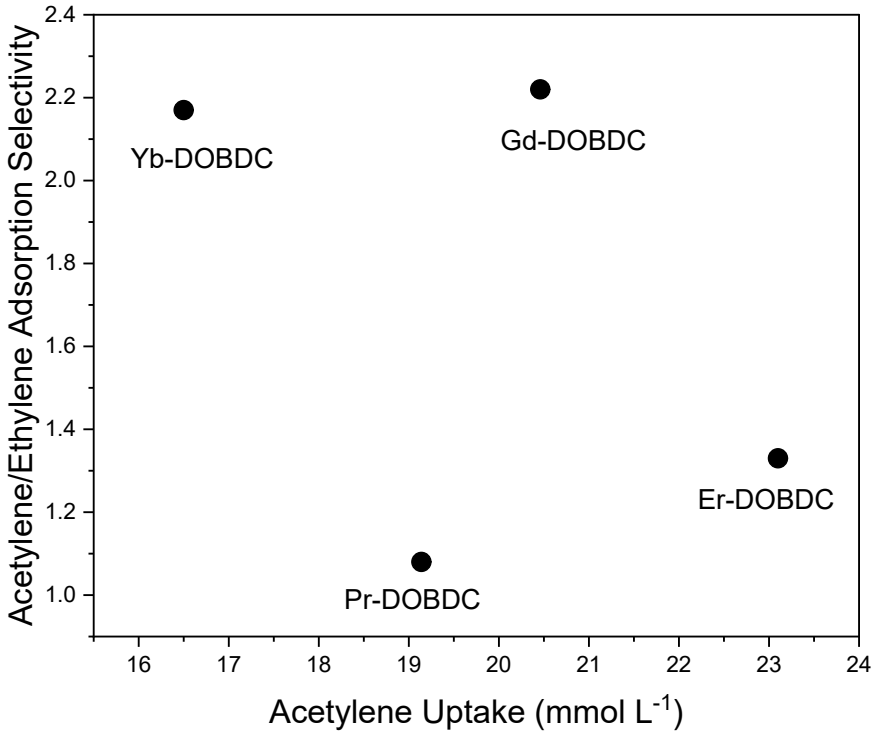

Figure 4. Acetylene/ethylene adsorption selectivity as a function of the acetylene uptake of Pr-, Gd-, Er-, and Yb-DOBDC in a 1 vol% acetylene/39 vol% ethylene, balance helium at 298 K.

Next, dynamic column breakthrough curve experiments were run using the Gd-DOBDC MOF, results included in Figure 5. The results show that despite the low acetylene concentration in the binary mixture (1 vol% acetylene), the acetylene has a longer retention time in the breakthrough column compared to ethylene. This data indicates that the separation of acetylene and ethylene can be achieved using the Gd-DOBDC MOF.

To accurately calculate the amount of acetylene adsorbed, blank breakthrough and desorption experiments were performed using blank columns with the same dimensions (and filled with quartz wool). The blank experiments were run under the same conditions as the sample breakthrough and desorption experiments. The normalized concentrations in the effluent stream during the desorption experiments are shown in Figure S6. It is reasonable to assume that acetylene and ethylene are adsorbed via physisorption and are completely desorbed during the desorption measurements. Thus, the amount adsorbed can be calculated by integrating the areas between the two desorption response curves without the effect of the roll-up during adsorption.

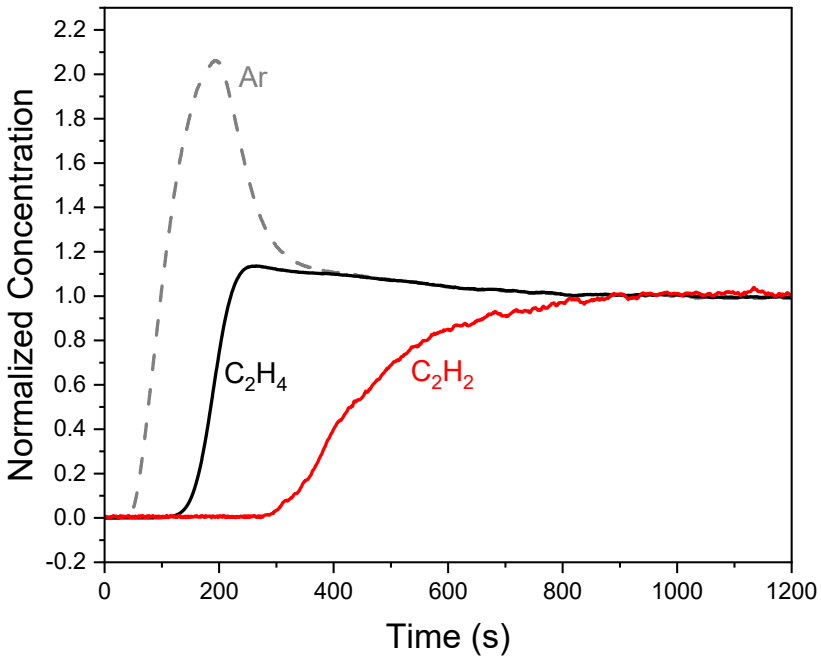

Figure 5. Fixed-bed breakthrough experiment response in Gd-DOBDC using 1 vol% acetylene/39 vol% ethylene, balance helium at 298K. The feed gas flowrate is 2 sccm.

3.5 Acetylene and Ethylene Diffusivity Experiments

In addition to the strength of the adsorption sites, diffusivity has been reported as a critical factor in kinetic separation performance of different MOFs.[40] In the RE-DOBDC MOFs studied here, the triangular window sizes are larger than 6 Å, while the kinetic diameters of acetylene and ethylene are 3.3 Å and 3.9 Å, respectively. Therefore, molecular sieving effects are not expected from the window and pore size decrease across the four MOFs studied. For that reason, the acetylene and ethylene diffusivities were measured to explore the effect of metal substitution on gas diffusivity in the isostructural MOFs.

The acetylene diffusivities were measured via ZLC using the 1 vol% acetylene / 39 vol% ethylene mixture. The results of this experiment are shown in Figure 6. The acetylene diffusivity was found to be the fastest in the Gd-DOBDC MOFs with a value of 7.1×10^{-15} m^2/s, and the diffusivities in the Er- and Yb-DOBDC MOFs are similar within experimental errors. The result indicates no dependency of acetylene diffusivity on the MOF window size. The estimated diffusion

selectivities are minimal and suggest that the separation is largely occurring via the strength of the individual gas binding sites, rather than diffusion of the gas molecules through the MOF

The ethylene diffusivity measured using the same acetylene/ethylene mixture is shown in Figure S7. The ethylene diffusivity is the fastest in the Gd-DOBDC MOF among the four MOFs studied with a value of 6.5×10^{-15} m^2/s. Similar to acetylene, no window size dependency was seen in ethylene diffusivities.

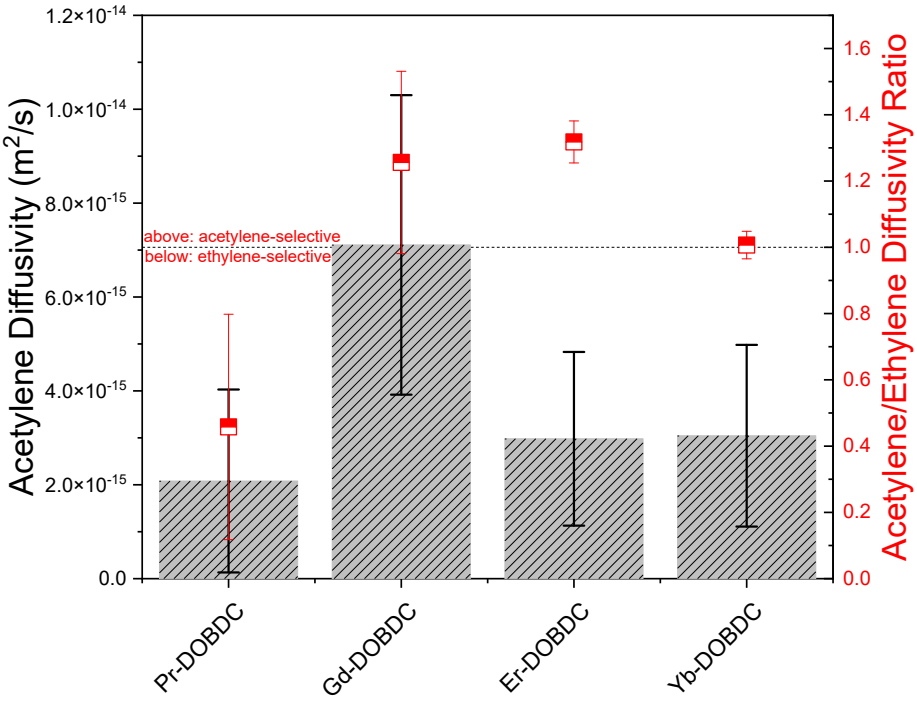

Figure 6. Mixture acetylene diffusivity (gray bars) and acetylene/ethylene diffusivity ratio (red square points) in Pr-, Gd-, Er-, and Yb-DOBDC, in order of decreasing pore size, measured at 298K and 1 bar using a 1/39 v/v acetylene/ethylene mixture. The total concentration of acetylene and ethylene is 5 vol%, with helium as a balance gas. The error bars reflect the variation in slope determination from the long-time asymptotes of the ZLC response curve.

4. Discussion

Understanding the complex mechanisms that control gas binding in porous materials requires leveraging multiple scientific techniques, including simulation and experiment. In this study, DFT simulations of gas binding sites as well as experimental gas adsorption isotherms and

diffusivities are used to evaluate ethylene/acetylene separations through a series of isostructural RE-DOBDC MOFs. By using isostructural porous materials, specific structural features that provide the largest impact on gas separations can be identified for future design of new and improved gas separation materials for targeted gas streams.

Interestingly, both the simulation and experimental results agree that the Yb-DOBDC MOF has the lowest adsorption capacity driven by the weakest binding energy with the acetylene and the ethylene molecules. Analysis of the Yb-DOBDC MOF structure identified that this MOF composition has the narrowest O-M-O bond angle between the two linkers and the metal in the cluster, resulting in the longest acetylene-metal interatomic distance and the weakest calculated gas binding energies. Narrow O-M-O distances sterically limit the accessibility of the metal cluster and decrease the available pore space, both of which limit gas adsorption.

Additionally, the absolute pressure of the gas in the experiments can affect the gas uptake and create challenges when comparing simulation data and experiment. Based on the DFT simulations of ethylene binding energies, the predicted gas adsorption trend for ethylene should be Pr > Gd > Er > Yb. However, at 100 kPa the gas adsorption capacity exhibits the following trend: Er > Gd > Pr > Yb. But at 10 kPa the adsorption capacity of the Gd- and Er-DOBDC MOFs are flipped: Gd > Er > Pr > Yb and at even pressures lower than 3 kPa the trend changes again to Gd > Pr > Er > Yb (see Figure 3). As the pressure in the isotherm adsorption data drops, the results become more consistent with the simulation data. The molecular scale simulations only include a single gas molecule, making comparison with low pressure gas adsorption experiments more representative of the simulation conditions. Moreover, additional effects such as gas-gas interactions and pore sizes are likely to be a factor at higher pressure, which would alter the adsorption mechanisms. These effects can be evaluated computationally but requires larger scale simulation methods such as classical molecular dynamics to capture these effects.

For acetylene, the simulated binding energy and experimental gas adsorption data is more consistent. Experimentally acetylene uptake follows the following trend Er > Gd > Pr > Yb, compared with the following simulated acetylene binding energy trends: Gd > Er > Pr > Yb. This may be due to the smaller size of the acetylene molecule, which allows it to access more pore space and stronger binding sites with or near the metal center, and fewer competing adsorption mechanisms such as hydrogen bonding with the DOBDC linker.

Regarding selectivity, the comparison between simulation and experimental results can be even more challenging, since changes in gas adsorption uptake occur at different pressures, as seen in Figure 3. However, using computational methods, the difference in the binding energies provide insight into sources of selectivity based on binding with or near the metal center. The predicted selectivity trend is Gd > Er > Yb > Pr. Data in Figure 3 for experimental acetylene/ethylene adsorption selectivity identifies the following trend: Gd > Yb > Er > Pr. Here the simulations have captured the end members, with stronger acetylene binding over ethylene in the Gd-DOBDC MOF and almost no difference in acetylene versus ethylene binding in the Pr-DOBDC MOF. This suggests that for the highest and lowest selectivity, the strength of the binding site is the dominate mechanism. In contrast, at intermediate selectivities for Yb- and Er-DOBDC MOFs, competitive adsorption effects may be more pronounced, and these effects can be difficult to capture computationally.

The combination of molecular scale simulation combined with experimental results is a powerful method for understanding interactions between gases and porous materials. That is clear for the current study of ethylene and acetylene adsorption in RE-DOBDC MOFs in which gas binding varies strongly with the O-M-O bond angle in the RE-DOBDC MOF for ethylene, but that hydrogen bonding with the hydroxyl on the DOBDC linker supports the stronger acetylene binding over ethylene. It is this finer understanding of the role of linker functionality and gas binding to the MOF framework that dominates the selectivity of acetylene gas over ethylene in these small pored RE-DOBDC MOFs, contrary to a more identifiable selectivity method of molecular sieving by pore size. Ultimately, molecular scale interactions with multiple aspects of the MOF, site accessibility, linker functionalization, porosity, and gas diffusivity are all critical to fully understanding how gases interact with porous functional materials.

5. Conclusion

In conclusion, this work investigated the acetylene/ethylene adsorption performance on four isostructural rare-earth DOBDC metal-organic frameworks (RE-DOBDC), each with substituted metal clusters. Inspired by previous literature showing the effect of MOF pore geometry on the acetylene/ethylene adsorption selectivity, this work studied the influence of metal-substitution in isostructural small pore RE-DOBDC (RE = Pr, Gd, Er, Yb) MOFs. The results proved to be more complex than initially surmised. The binding energies of acetylene and ethylene

were calculated using DFT simulations to identify mechanisms that control ethylene/acetylene adsorption and selectivity. DFT calculations showed that both acetylene and ethylene were stable in the RE-DOBDC MOFs, with higher acetylene adsorption in the Gd-, Er-, and Yb-DOBDC MOFs. Furthermore, structural analysis of acetylene binding revealed that the acetylene adsorption is dominated by hydrogen-bonding with the linker hydroxyl, while for ethylene binding is controlled by the linker geometry around the metal center. Direct interaction with the metal center does not play a major role in gas adsorption.

The experimental adsorption capacities were measured from single-component ethylene adsorption up to 1 bar and dynamic breakthrough experiments of 1 vol% acetylene/39 vol% ethylene mixture (with a balance of helium for safety considerations). The results showed that the Gd-DOBDC MOF had the highest acetylene adsorption capacity and acetylene/ethylene adsorption selectivity among the four MOFs studied. Findings from intracrystalline diffusivity measurements indicate that the acetylene diffusivity is influenced by the relative ethylene binding energy. As a result, greater differences in sorbate affinity result in enhanced diffusion selectivity. Low pressure gas adsorption experiments validated the modeling since the gas-MOF interactions are driven by the strength of gas binding sites within the MOF. At higher pressures the correlation between modeling and experiment begins to break down to secondary effects that only occur at higher pressures, such as gas-gas interactions and diffusivity of gases through the MOF framework.

Through evaluation of ethylene and acetylene adsorption with isostructural RE-DOBDC MOFs, mechanisms of gas adsorption based on interaction with the functionalization of the linker and linker geometry around the metal center was the driving force for selectivity. The results highlight the complexity of gas binding in porous functional materials and the critical role that combined modeling and experiment provide in developing a fundamental understanding of gas-framework interactions that can be leveraged for design of future separation materials.

Supporting Information

Supporting information includes a description of the zero-length column (ZLC) diffusivity analysis (Section S1), synthesis conditions for Gd-, Er-, and Yb-DOBDC MOFs (Section S2), optimized ME-DOBDC MOF unit cell dimensions (Table S1), simulated and experimental x-ray diffraction patterns (Figure S1-S3), set-up for the diffusivity measurement (Figure S4), snapshots of metal clusters in the simulated RE-DOBDC MOFs (Figure S5), normalized outlet acetylene and ethylene

concentration in fixed-bed desorption experiment of Gd- and Yb-DOBDC MOFs (Figure S6 and S8), mixed ethylene diffusivity measurements (Figure S7), and normalized outlet concentration in fixed-bed desorption experiments of Er- and Pr-DOBDC MOFs (Figure S9 and S10).

Author Information

Corresponding Author

*Jessica M. Rimsza – Geochemistry Department, Sandia National Laboratories, MS-0750 PO Box 5800, Albuquerque, NM, 87185, USA, jrimsza@sandia.gov
*Ryan P., Lively - School of Chemical & Biomolecular Engineering, Georgia Institute of Technology, 311 Ferst Dr., Atlanta, GA, 30332-0100, USA, ryan.lively@chbe.gatech.edu

Authors

Chunyi Li - School of Chemical & Biomolecular Engineering, Georgia Institute of Technology, 311 Ferst Dr., Atlanta, GA, 30332-0100, USA
Susan E. Henkelis – AO Sensing & EC Engineering Department, Sandia National Laboratories, Albuquerque, NM 87123 USA
Akriti Sarswat - School of Chemical & Biomolecular Engineering, Georgia Institute of Technology, 311 Ferst Dr., Atlanta, GA, 30332-0100, USA
Tina M. Nenoff - Advanced Science and Technology, Sandia National Laboratories, Albuquerque, New Mexico 87185, United States

Acknowledgment

This work was supported by the Center for Understanding and Controlling Accelerated and Gradual Evolution of Materials for Energy (UNCAGE-ME), an Energy Frontier Research Center funded by the U.S. Department of Energy, Office of Science, Office of Basic Energy Sciences, under Award No. DE-SC0012577. This article has been authored by an employee of National Technology & Engineering Solutions of Sandia, LLC, under Contract No. DE-NA0003525 with the U.S. Department of Energy (DOE). The employee owns all right, title, and interest in and to the article and is solely responsible for its contents. The United States Government retains and the publisher, by accepting the article for publication, acknowledges that the United States Government retains a non-exclusive, paid-up, irrevocable, world-wide license to publish or reproduce the published form of this article or allow others to do so, for United States Government purposes. The DOE will provide public access to these results of federally sponsored research in

accordance with the DOE Public Access Plan https://www.energy.gov/downloads/doe-public-access-plan.

CRediT Author Statement

Chunyi Li: methodology, formal analysis, investigation, data curation, writing – original draft, visualization, **Akriti Sarswat**: methodology, formation analysis, investigation, writing – original draft, writing – review & editing, **Susan E. Henkelis**: conceptualization, methodology, resources, writing, review & editing, **Tina M. Nenoff**: conceptualization, resources, writing – review & editing, supervision, project administration, funding acquisition, **Ryan P. Lively**: conceptualization, resources, writing – review & editing, supervision, project administration, funding acquisition, **Jessica M. Rimsza**: methodology, software, formation analysis, investigation, data curation, writing – original draft, writing – review & editing, visualization, project administration

References

1.Chauhan, R.; Sartape, R.; Minocha, N.; Goyal, I.; Singh, M. R., Advancements in environmentally sustainable technologies for ethylene production. *Energ. Fuel.* **2023,** *37* (17), 12589-12622.

2. Ren, T.; Patel, M.; Blok, K., Olefins from conventional and heavy feedstocks: Energy use in steam cracking and alternative processes. *Energy* **2006,** *31* (4), 425-451.

3. Gao, Y.; Neal, L.; Ding, D.; Wu, W.; Baroi, C.; Gaffney, A. M.; Li, F., Recent advances in intensified ethylene production—a review. *ACS Catalysis* **2019,** *9* (9), 8592-8621.

4. Gu, X.-W.; Pei, J.; Shao, K.; Wen, H.-M.; Li, B.; Qian, G., Chemically stable hafnium-based metal–organic framework for highly efficient C_2H_6/C_2H_4 separation under humid conditions. *ACS Appl. Mater. Interfaces* **2021,** *13* (16), 18792-18799.

5. Li, L.; Krishna, R.; Wang, Y.; Wang, X.; Yang, J.; Li, J., Flexible metal–organic frameworks with discriminatory gate - opening effect for the separation of acetylene from ethylene/acetylene mixtures. *Eur. J. Inorg. Chem.* **2016,** *2016* (27), 4457-4462.

6. Molero, H.; Bartlett, B.; Tysoe, W., The hydrogenation of acetylene catalyzed by palladium: hydrogen pressure dependence. *J. Catal.* **1999,** *181* (1), 49-56.

7. Aguado, S.; Bergeret, G.; Daniel, C.; Farrusseng, D., Absolute molecular sieve separation of ethylene/ethane mixtures with silver zeolite A. *J. Amer. Chem. Soc.* **2012,** *134* (36), 14635-14637.

8. Wen, H.-M.; Li, B.; Wang, H.; Krishna, R.; Chen, B., High acetylene/ethylene separation in a microporous zinc (II) metal–organic framework with low binding energy. *Chem. Commun.* **2016,** *52* (6), 1166-1169.

9. Das, M. C.; Guo, Q.; He, Y.; Kim, J.; Zhao, C.-G.; Hong, K.; Xiang, S.; Zhang, Z.; Thomas, K. M.; Krishna, R., Interplay of metalloligand and organic ligand to tune micropores within isostructural mixed-metal organic frameworks (M′ MOFs) for their highly selective separation of chiral and achiral small molecules. *J. Amer. Chem. Soc.* **2012,** *134* (20), 8703-8710.

10. He, Y.; Krishna, R.; Chen, B., Metal–organic frameworks with potential for energy-efficient adsorptive separation of light hydrocarbons. *Energy Environ. Sci.* **2012,** *5* (10), 9107-9120.

11. Bloch, E. D.; Queen, W. L.; Krishna, R.; Zadrozny, J. M.; Brown, C. M.; Long, J. R., Hydrocarbon separations in a metal-organic framework with open iron (II) coordination sites. *Science* **2012,** *335* (6076), 1606-1610.

12. Hu, T.-L.; Wang, H.; Li, B.; Krishna, R.; Wu, H.; Zhou, W.; Zhao, Y.; Han, Y.; Wang, X.; Zhu, W., Microporous metal–organic framework with dual functionalities for highly efficient removal of acetylene from ethylene/acetylene mixtures. *Nat. Commun.* **2015,** *6* (1), 7328.

13. Lin, R.-B.; Li, L.; Wu, H.; Arman, H.; Li, B.; Lin, R.-G.; Zhou, W.; Chen, B., Optimized separation of acetylene from carbon dioxide and ethylene in a microporous material. *J. Amer. Chem. Soc.* **2017,** *139* (23), 8022-8028.

14. Li, B.; Cui, X.; O'Nolan, D.; Wen, H. M.; Jiang, M.; Krishna, R.; Wu, H.; Lin, R. B.; Chen, Y. S.; Yuan, D., An ideal molecular sieve for acetylene removal from ethylene with record selectivity and productivity. *Adv. Mater.* **2017,** *29* (47), 1704210.

15. Cui, X.; Chen, K.; Xing, H.; Yang, Q.; Krishna, R.; Bao, Z.; Wu, H.; Zhou, W.; Dong, X.; Han, Y., Pore chemistry and size control in hybrid porous materials for acetylene capture from ethylene. *Science* **2016,** *353* (6295), 141-144.

16. Henkelis, S. E.; Judge, P. T.; Hayes, S. E.; Nenoff, T. M., Preferential SOx adsorption in Mg-MOF-74 from a humid acid gas stream. *ACS Appl. Mater. Interfaces* **2021,** *13* (6), 7278-7284.
17. Henkelis, S. E.; Vogel, D. J.; Metz, P. C.; Valdez, N. R.; Rodriguez, M. A.; Rademacher, D. X.; Purdy, S.; Percival, S. J.; Rimsza, J. M.; Page, K., Kinetically controlled linker binding in rare earth-2, 5-dihydroxyterepthalic acid metal–organic frameworks and its predicted effects on acid gas adsorption. *ACS Appl. Mater. Interfaces* **2021,** *13* (47), 56337-56347.
18. Gallis, D. F. S.; Rohwer, L. E.; Rodriguez, M. A.; Barnhart-Dailey, M. C.; Butler, K. S.; Luk, T. S.; Timlin, J. A.; Chapman, K. W., Multifunctional, tunable metal-organic framework materials platform for bioimaging applications. *ACS Appli. Mater. Interfaces* **2017,** *9* (27), 22268-22277.
19. Sava Gallis, D. F.; Vogel, D. J.; Vincent, G. A.; Rimsza, J. M.; Nenoff, T. M., NO x adsorption and optical detection in rare earth metal–organic frameworks. *ACS Appl. Mater. Interfaces* **2019,** *11* (46), 43270-43277.
20. Christian, M. S.; Fritzsching, K. J.; Harvey, J. A.; Sava Gallis, D. F.; Nenoff, T. M.; Rimsza, J. M., Dramatic Enhancement of Rare-Earth Metal–Organic Framework Stability Via Metal Cluster Fluorination. *J. Amer. Chem. Soc. Au* **2022,** *2* (8), 1889-1898.
21. Vogel, D. J.; Lee, Z. R.; Hanson, C. A.; Henkelis, S. E.; Smith, C. M.; Nenoff, T. M.; Dixon, D. A.; Rimsza, J. M., Predictive acid gas adsorption in rare earth DOBDC metal–organic frameworks via complementary cluster and periodic structure models. *J. Phys. Chem. C* **2020,** *124* (49), 26801-26813.
22. Kresse, G.; Hafner, J., Ab initio molecular-dynamics simulation of the liquid-metal–amorphous-semiconductor transition in germanium. *Phys. Rev. B* **1994,** *49* (20), 14251.
23. Kresse, G.; Hafner, J., Ab initio molecular dynamics for liquid metals. *Phys. Rev. B* **1993,** *47* (1), 558.
24. Kresse, G.; Furthmüller, J., Efficiency of ab-initio total energy calculations for metals and semiconductors using a plane-wave basis set. *Comput. Mater. Sci.* **1996,** *6* (1), 15-50.
25. Blöchl, P. E., Projector augmented-wave method. *Phys. Rev. B* **1994,** *50* (24), 17953.
26. Kresse, G.; Joubert, D., From ultrasoft pseudopotentials to the projector augmented-wave method. *Phys. Rev. B* **1999,** *59* (3), 1758.
27. Perdew, J. P.; Ruzsinszky, A.; Csonka, G. I.; Vydrov, O. A.; Scuseria, G. E.; Constantin, L. A.; Zhou, X.; Burke, K., Restoring the density-gradient expansion for exchange in solids and surfaces. *Phys. Rev. Lett.* **2008,** *100* (13), 136406.
28. Vogel, D. J.; Nenoff, T. M.; Rimsza, J. M., Tuned hydrogen bonding in rare-earth metal–organic frameworks for design of optical and electronic properties: an exemplar study of Y–2, 5-dihydroxyterephthalic acid. *ACS Appl. Mater. Interfaces* **2020,** *12* (4), 4531-4539.
29. Grimme, S.; Antony, J.; Ehrlich, S.; Krieg, H., A consistent and accurate ab initio parametrization of density functional dispersion correction (DFT-D) for the 94 elements H-Pu. *J. Chem. Physics* **2010,** *132* (15).
30. Grimme, S.; Ehrlich, S.; Goerigk, L., Effect of the damping function in dispersion corrected density functional theory. *J. Comput. Chem.* **2011,** *32* (7), 1456-1465.
31. Vogel, D. J.; Gallis, D. F. S.; Nenoff, T. M.; Rimsza, J. M., Structure and electronic properties of rare earth DOBDC metal–organic-frameworks. *Phys. Chem. Chem. Phys.* **2019,** *21* (41), 23085-23093.

32. Vizuet, J. P.; Mortensen, M. L.; Lewis, A. L.; Wunch, M. A.; Firouzi, H. R.; McCandless, G. T.; Balkus Jr, K. J., Fluoro-Bridged Clusters in Rare-Earth Metal–Organic Frameworks. *J. Amer. Chem. Soc.* **2021,** *143* (43), 17995-18000.
33. Parkes, M. V.; Sava Gallis, D. F.; Greathouse, J. A.; Nenoff, T. M., Effect of metal in M3 (btc) 2 and M2 (dobdc) MOFs for O_2/N_2 separations: a combined density functional theory and experimental study. *J. Phys. Chem. C* **2015,** *119* (12), 6556-6567.
34. Ruthven, D.; Loughlin, K., The effect of crystallite shape and size distribution on diffusion measurements in molecular sieves. *Chem. Eng. Sci.* **1971,** *26* (5), 577-584.
35. Eic, M.; Ruthven, D. M., A new experimental technique for measurement of intracrystalline diffusivity. *Zeolites* **1988,** *8* (1), 40-45.
36. Ruthven, D. M.; Brandani, S., Measurement of diffusion in porous solids by zero length column (ZLC) methods. In *Membrane science and technology*, Elsevier: 2000; Vol. 6, pp 187-212.
37. Taylor, R.; Kennard, O., Hydrogen-bond geometry in organic crystals. *Acc. Chem. Res.* **1984,** *17* (9), 320-326.
38. Hartmann, M.; Wetmore, S. D.; Radom, L., C− H⊙⊙⊙ X Hydrogen Bonds of Acetylene, Ethylene, and Ethane with First-and Second-Row Hydrides. *J. Phys. Chem. A* **2001,** *105* (18), 4470-4479.
39. Scheiner, S.; Grabowski, S. J.; Kar, T., Influence of Hybridization and Substitution on the Properties of the CH⊙⊙⊙ O Hydrogen Bond. *J. Phys. Chem. A* **2001,** *105* (46), 10607-10612.
40. Krokidas, P.; Castier, M.; Economou, I. G., Computational study of ZIF-8 and ZIF-67 performance for separation of gas mixtures. *J. Phys. Chem. C* **2017,** *121* (33), 17999-18011.

Table of Contents Graphic: